Patching sulfur vacancies

A versatile approach for achieving ultrasensitive gas sensors based on transition metal dichalcogenides

Liu, Xiangcheng; Niu, Yue; Jin, Duo; Zeng, Junwei; Li, Wanjiang; Li, Hao; Lee, Yi Kuen; French, Paddy J.; Wang, Yao; More Authors

DOI
10.1016/j.jcis.2023.06.092

Publication date
2023

Document Version
Final published version

Published in
Journal of Colloid and Interface Science

Journal of Colloid and Interface Science 649 (2023) 909–917

Contents lists available at ScienceDirect

Journal of Colloid And Interface Science

journal homepage: www.elsevier.com/locate/jcis

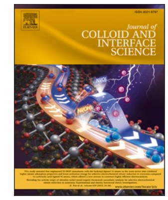

Patching sulfur vacancies: A versatile approach for achieving ultrasensitive gas sensors based on transition metal dichalcogenides

Xiangcheng Liu [a], Yue Niu [a,b,*], Duo Jin [a], Junwei Zeng [a], Wanjiang Li [a], Lirong Wang [c], Zhipeng Hou [c], Yancong Feng [a], Hao Li [a], Haihong Yang [d], Yi-Kuen Lee [e], Paddy J. French [f], Yao Wang [a,*], Guofu Zhou [a]

[a] *Guangdong Provincial Key Laboratory of Optical Information Materials and Technology, Institute of Electronic Paper Displays, South China Academy of Advanced Optoelectronics, South China Normal University, Guangzhou 510006, PR China*
[b] *School of Physical Sciences, Great Bay University, Dongguan 523000, PR China*
[c] *Guangdong Provincial Key Laboratory of Optical Information Materials and Technology & Institute for Advanced Materials, South China Academy of Advanced Optoelectronics South China Normal University, Guangzhou 510006, PR China*
[d] *Department of Thoracic Oncology, State Key Laboratory of Respiratory Diseases, The First Affiliated Hospital of Guangzhou Medical University, Guangzhou 510006, PR China*
[e] *Department of Mechanical & Aerospace Engineering, Hong Kong University of Science and Technology, Clear Water Bay, Kowloon, Hong Kong Special Administrative Region*
[f] *BE Laboratory, EWI, Delft University of Technology, Delft 2628CD, the Netherlands*

HIGHLIGHT

- Covalently patched the sulfur vacancies of Transition Metal Dichalcogenides, which decreased the density of surface defect and improved its NO_2 sensing performance.
- The Fermi-level of 4-nitrothiophenol healed MoS_2 shift toward the valence band demonstrate the *n*-doping process, thereby increased the carriers of MoS_2.
- 4-nitrothiophenol healed MoS_2 performed a higher NO_2 response (increased by 200 %) and lower limit of detection (10 ppb).

GRAPHICAL ABSTRACT

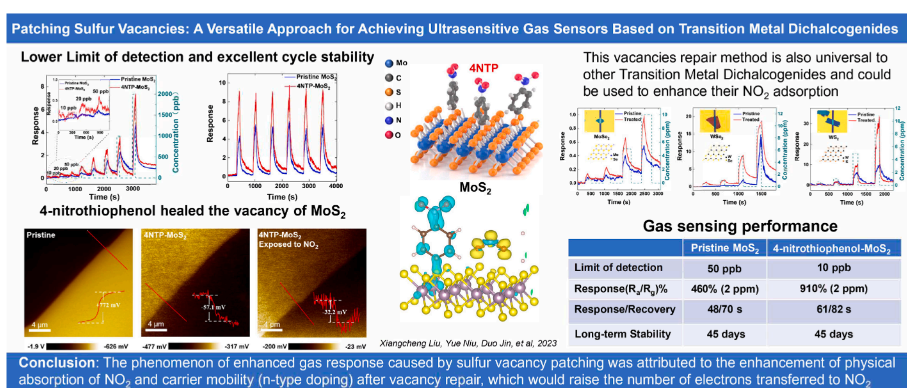

ARTICLE INFO

Keywords:
2D materials
Transition metal dichalcogenides
Gas sensing
Patching sulfur vacancies
N-doping

ABSTRACT

Transition metal dichalcogenides (TMDCs) garner significant attention for their potential to create high-performance gas sensors. Despite their favorable properties such as tunable bandgap, high carrier mobility, and large surface-to-volume ratio, the performance of TMDCs devices is compromised by sulfur vacancies, which reduce carrier mobility. To mitigate this issue, we propose a simple and universal approach for patching sulfur vacancies, wherein thiol groups are inserted to repair sulfur vacancies. The sulfur vacancy patching (SVP) approach is applied to fabricate a MoS_2-based gas sensor using mechanical exfoliation and all-dry transfer

* Corresponding authors.
E-mail addresses: niuyue@gbu.edu.cn (Y. Niu), wangyao@m.scnu.edu.cn (Y. Wang).

https://doi.org/10.1016/j.jcis.2023.06.092
Received 27 April 2023; Received in revised form 7 June 2023; Accepted 14 June 2023
Available online 17 June 2023

methods, and the resulting 4-nitrothiophenol (4NTP) repaired molybdenum disulfide (4NTP-MoS_2) is prepared via a sample solution process. Our results show that 4NTP-MoS_2 exhibits higher response (increased by 200 %) to ppb-level NO_2 with shorter response/recovery times (61/82 s) and better selectivity at 25 °C compared to pristine MoS_2. Notably, the limit of detection (LOD) toward NO_2 of 4NTP-MoS_2 is 10 ppb. Kelvin probe force microscopy (KPFM) and density functional theory (DFT) reveal that the improved gas sensing performance is mainly attributed to the 4NTP-induced *n*-doping effect on MoS_2 and the corresponding increment of surface absorption energy to NO_2. Additionally, our 4NTP-induced SVP approach is universal for enhancing gas sensing properties of other TMDCs, such as $MoSe_2$, WS_2, and WSe_2.

1. Introduction

Two-dimensional (2D) materials, especially transition metal chalcogenides (TMDCs), possess the characteristics of adjustable band gap, carrier mobility, large specific surface area, etc. [1,2], and have immense potential in the broad fields of optoelectronics [3–5], logic electronics [6], and sensors [7–9]. In recent years, researchers have found that the interaction between 2D materials and gas molecules can be significantly affected by the surface chemical state of 2D materials [10–13]. Therefore, their gas sensing performances could be modulated by modifying diverse organic molecules on the surface [14–17]. In general, the surface of TMDCs could be modified by organic molecules via covalent bonds [18,19] and non-covalent bonds [20,21]. Although non-covalent bond modification can promptly and non-destructively form a highly ordered molecular film on the surface of TMDCs, it is brittle to the change of external environments (such as humidity and stress), due to their weak binding strength between organic molecules and the surface of TMDCs [22]. The other approach is to modify TMDCs via covalently bonding. Recent research mainly used diazo compounds [23], olefins [24], and thiol sulfur compounds [25] to form C—S covalent bonds on the surface of TMDCs. However, most of these methods have to suffer violent chemical reactions, which could easily lead to phase transition of TMDCs, causing the decline of their semiconductor performance and hindering their application in the field of gas sensors.

Compare with the above methods, bonding organic molecules containing sulfhydryl groups with the sulfur vacancies generated during the preparation of TMDCs would only affect the surface state of TMDCs and consequently maintain the semiconductor properties of TMDCs [18,26,27]. In 2012, Makarova et al. [28] employed two thiol-contained organic molecules (3-mercaptopropyl-trimethylsilane and dodecanethiol) to modify MoS_2 and found by scanning tunneling microscopy (STM) that chemical bonds rather than simple physical adsorption were formed between the thiol group and the sulfur vacancies on the surface of MoS_2. Bertozzi et al. [29] treated MoS_2 monolayer by vapor deposition method. Short-chain alkane thiols (butyl mercaptan) were evaporated on the surface and bonded with the defects of MoS_2. The repairing effect of thiol groups to the surface defects of TMDCs has been verified by fluorescence and Raman spectroscopy [30]. Meanwhile, by adjusting the species of organic molecules with thiol groups, the doping degree of organic molecules to TMDCs can also be effectively regulated [25,31]. With abundant alternative functional groups and π-conjugated electron transport channels, thiophenol derivatives have become a powerful candidate for covalently functionalized TMDCs. Paolo et al. utilized benzene 1,4-dithiol to bridge the adjacent MoS_2 flakes through vacancies [32], which significantly promoted the interlayer charge transport of MoS_2, and dramatically improved the carrier mobility and I_{on}/I_{off} ratio of MoS_2, reaching $10^{-2} cm^2V^{-1}s^{-1}$, 10^4, respectively. Sunkook et al. significantly improved the current and carrier concentration of MoS_2 through functionalizing MoS_2 by sulfur vacancies using thiophenol derivatives [25]. Besides, as for other 2D materials, Xu et al. fabricated chemiresistive gas sensors using thiophenol derivatives functionalized organic-metal chalcogenides, and realized an 852.6 % (I_g/I_a) response to 10 ppm NO_2 at room-temperature [33]. In summary, thiophenol derivatives can be used to effectively modify the surface of TMDCs through repairing their sulfur vacancies with covalent bonds and their electrical properties could be regulated by altering the species of terminal groups in thiophenol derivatives [17,31]. Although a series of studies have devoted on SVP of TMDCs, most of them have only focused on the modification methodology and related physical properties [22]. As another important application, the effects of SVP on the gas sensing performance of TMDCs have not been studied so far.

In this work, we repaired sulfur vacancies on mechanically exfoliated TMDCs including MoS_2, $MoSe_2$, WS_2, and WSe_2, and exceedingly improved their gas sensing properties with a new approach of SVP using π-conjugated p-nitrothiophenol (4NTP). Both experimental method analysis and theoretical calculations demonstrated that 4NTP successfully patched the sulfur vacancies of TMDCs, and the NO_2 response enhancement of TMDCs is attributed to the *n*-type doping effect. The increasing number of carriers and the reduction of charge scattering centers ultimately enhance the gas sensing response of the TMDCs. The 4NTP-MoS_2 devices exhibited superior gas sensing performance toward NO_2 (limit of detection is 10 ppb) among the reported TMDCs-based gas sensors so far.

2. Experimental section

2.1. Preparation of MoS_2, $MoSe_2$, WS_2, and WSe_2 nanosheets

The mechanical exfoliation method was used to obtain MoS_2 nanosheets from the bulk MoS_2 crystals (SixCarbon Technology Shenzhen, China). To begin with, a piece of Nitto tape (Nitto Denko, Japan, SPV 224P) was adhered to MoS_2 crystal and gently peeled off. Then a translucent poly(dimethylsiloxane) (PDMS) stamp (Gel-Pak, USA, WF-30-X4) was covered tightly on the MoS_2 sheets. By carefully removing the stamp, the MoS_2 nanosheets could be stuck to the PDMS ultimately. The $MoSe_2$, WS_2, and WSe_2 nanosheets were obtained by the same approach.

2.2. Fabrication of gas sensors

The inspection and selection of the MoS_2 nanosheets were operated on a polarization microscope (Leica Microsystems, Germany, DM2700P). Then, by an all-dry transfer method, which transferred MoS_2 nanosheets from the PDMS stamp to the Cr (5 nm)/Au (60 nm) electrodes pre-patterned on the SiO_2 (280 nm)/Si wafer, the MoS_2-based gas sensor was successfully fabricated. Other TMDCs-Based gas sensors were prepared similarly.

2.3. Sulfur vacancy patching

For thiophenol-based patching, 4NTP (96 %, Alfa Aesar) was dissolved in DMSO (99.9 %, Innochem) and ultrasonicated for 10 min. To repair sulfur vacancies of MoS_2, 10 μL of 0.02 mol/L 4NTP, were lightly dropped onto the MoS_2-based gas sensors. After being treated for 6 h, the MoS_2-based gas sensors were washed by DMSO 3 times to rinse extra organic molecules. Then, eventually, they were dried in a vacuum oven for 2 h under 60 °C.

 Journal of Colloid And Interface Science 649 (2023) 909–917

2.4. Characterization

All the optical images were acquired by DM2700P polarization microscope under the reflection mode. AFM characterization was operated in ScanAsyst mode on an atomic force microscope (Bruker, USA, Multimode 8) using SCANASYST-AIR probes and KPFM characterization was conducted in the electronic and magnetic lift mode on the same apparatus using SCM-PIT-V2 probes. Confocal Raman and PL spectra were measured with the Raman microscope (RENISHAW, UK, inVia) under a 532 nm excitation wavelength before and after injecting the NO_2 gas in a quartz chamber. XPS measurements were performed in an ultravacuum vessel in a Thermo Fisher Scientific Escalab 250Xi using an Al Kα excitation source.

2.5. Gas sensing properties tests

All the gas sensing tests were carried out in the same environment at room temperature (25 °C) and a stabilized certain relative humidity range (25–30 %) using a home-built gas sensing system. Light-enhanced gas sensing method was used to acquire a swift response and recovery

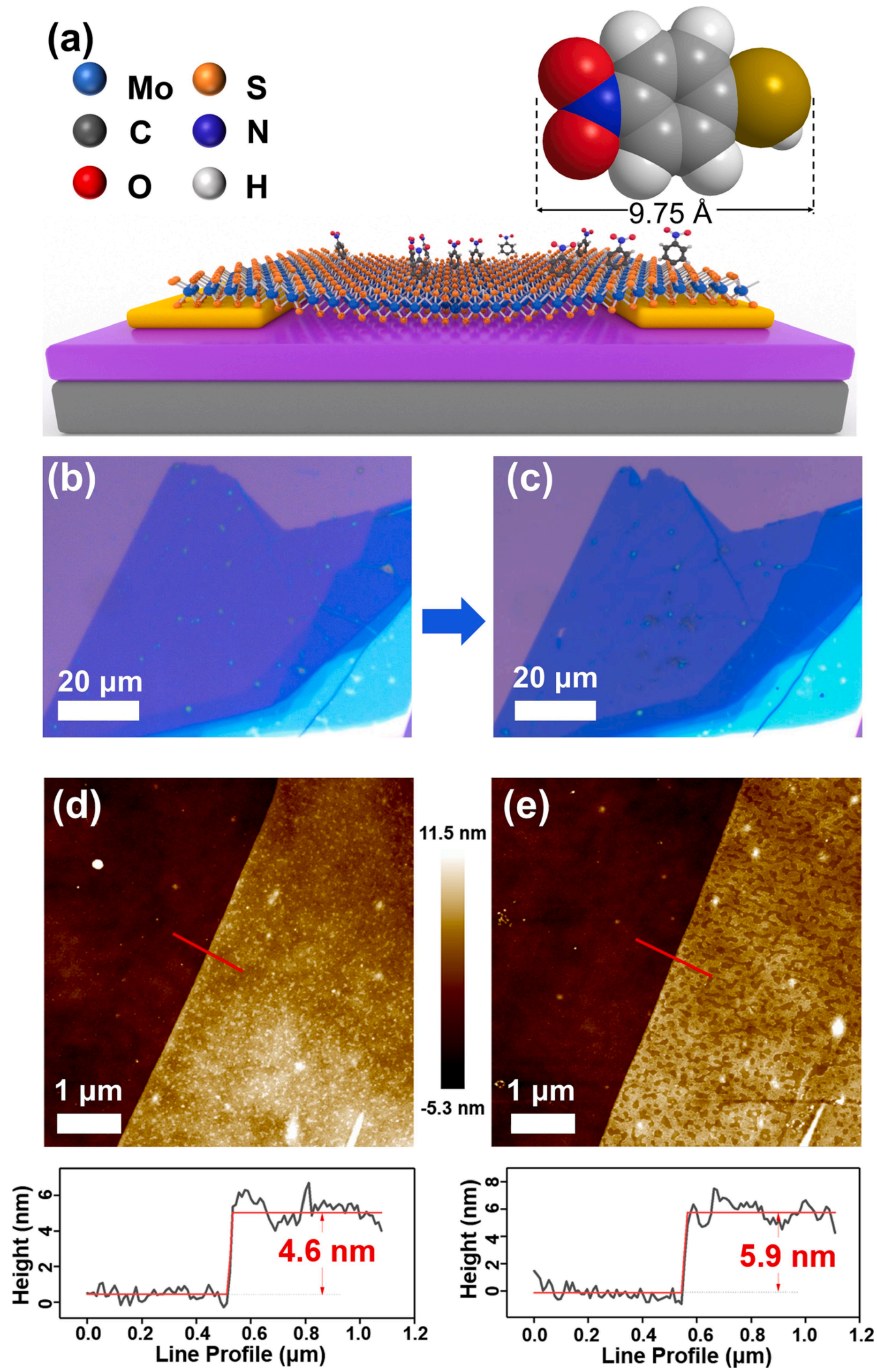

Fig. 1. (a) Schematic illustration of MoS_2 after SVP. (b), (c) Optical images of the pristine MoS_2 and 4NTP- MoS_2 nanosheets. (d), (e) Corresponding AFM images of the pristine MoS_2 and 4NTP-MoS_2 nanosheets from (b) and (c), and the illustration of the line scan for specific data.

time using a light-emitting diode (LED) light source. The power density of LED was calibrated using a silicon photodiode sensor (Thorlabs, USA, S120VC). The relevant electrical measurements were performed utilizing Keithley 2450 source meter (Tektronix).

2.6. Density functional theory calculation

This work was performed using the Vienna Ab initio Simulation Package (VASP). We have employed first-principles to perform DFT calculations within the generalized gradient approximation using the Perdew–Burke–Ernzerhof formulation. To avoid interactions among layers, we built a vacuum space larger than 20 Å for the crystal structure. The cutoff energy was adopted as 400 eV, and the BZ was sampled with a Γ-centered k-point mesh of 5 × 3 × 1. The electronic energy was considered self-consistent when the energy change was smaller than 10^{-4} eV. In the calculation, the convergence criterion of the force is set to 0.01 eV $Å^{-1}$. The DFT-D2 method was used to consider the long-range van der Waals interactions.

3. Results and discussion

The TMDCs-Based gas sensors were fabricated from the bulk TMDCs crystals through mechanical exfoliation and all-dry transfer onto Cr/Au electrodes [34]. Unlike the ideal regular surface, a certain amount of sulfur vacancies are inevitably introduced on the surface and edge of TMDCs during exfoliation [31,35], which would reduce the carrier density and mobility of the material, thereby affecting device performance. Through SVP engineering, the electronic and chemical properties of the material can be strategically altered or improved [36]. In this research, 4NTP, a typical thiophenol ramification, was selected as SVP candidate, whose nitro group has strong electron-withdrawing induction effect and electron-withdrawing conjugation effect. In dimethyl sulfoxide (DMSO) solution, the nitro group can delocalize the negative charge of the sulfhydryl anion to its oxygen atom which produces corresponding anion and then form the S—C bond with high-activity sulfur vacancies [25,37].

3.1. Morphology and spectroscopic characterization

As shown in Fig. 1**a, b and c**, SVP was performed by dropping the 4NTP onto the MoS_2-based gas sensors (4NTP-MoS_2), and the optical image of 4NTP treated MoS_2 performed no obvious difference from pristine MoS_2. Fig. 1**d and e** show atomic force microscopy (AFM) images of MoS_2 before and after SVP in a 20 mM 4NTP solution for 6 h, respectively. It is noticed that the height of MoS_2 nanosheet increases about 1.3 nm (from ~4.6 nm to ~5.9 nm), which is close to the size of 4NTP molecular (9.75 Å [38]) and is consistent with the reports of the 2D materials covalent functionalization [23,39,40].

To prove the thiophenol derivatives have successfully repaired the vacancies of TMDCs, we adopted a series of spectral characterizations to confirm the changes before and after SVP. As shown in Raman spectra (Fig. 2**a**), the in-plane A_{1g} mode at 407.2 cm^{-1} and the out-of-plane E^1_{2g} mode at 382.2 cm^{-1} of pristine MoS_2 were measured. Compared to the pristine MoS_2, the modification of 4NTP promoted redshift which corresponded to the improvement of the electron concentration owing to the increased electron–phonon scattering [41]. The 4NTP-MoS_2 induced redshift of 0.318 and 0.627 cm^{-1} respectively, indicating *n*-doping [23]. The obtained Raman test results keep in line with our following KPFM measurements and DFT calculation in the follow-up discussion, which provided a shred of explicit evidence that *n*-doping happened to 4NTP-MoS_2. The PL spectra (Fig. 2**b**) of 4NTP-MoS_2 showed an obvious redshift from 677.84 nm to 679.73 nm, which is generally ascribed to the *n*-doping from 4NTP or the elimination of p-type absorbates like O_2 or H_2O [42–46]. Considering most of the O_2 or H_2O has been removed by our vacuum drying procedure, it is believed that the SVP predominated PL spectrum redshift.

Micro-area X-ray photoelectron spectroscopy (XPS) was applied to characterize the chemical bond state of MoS_2 and 4NTP-MoS_2. The relevant 4NTP C 1 s XPS signal of the 4NTP-MoS_2 (Fig. 2**c**) was constructed of C—NO_2 bond and C—S bond, located at 288.5–289.5 and 286–287.5 eV.[47] Compared to the pristine MoS_2, the 4NTP-MoS_2 after SVP possesses a distinct C-NO_2 peak centered at 289.18 eV, which successfully proved the existence of the C—N bond from 4NTP. Moreover, the presence of N—C and N—O verified the existence of 4NTP on MoS_2 (Fig. 4**a, b**).

3.2. NO_2 gas sensing properties

The gas sensing experiments of pristine MoS_2 and 4NTP-MoS_2 were performed by a sophisticated home-built gas sensing system.[48] To minimize the baseline oscillation and accelerate the response/recovery speed (**Figure S2**), a 405 nm light source was applied to improve gas sensing performance. Fig. 3**a** shows the gas sensing performance of the pristine MoS_2 and 4NTP-MoS_2 with a NO_2 concentration gradient under 12 mW/cm^2 405 nm light illumination. The gas sensing response of the sensors is defined as Equation (1):

$$Response = \frac{(R_g - R_a)}{R_a} \quad (1)$$

where R_g is the resistance of gas sensors exposed to the NO_2 atmosphere and R_a is the resistance around the baseline. Fig. 3a illustrates the dynamic response of the pristine MoS_2 and 4NTP-MoS_2, with the NO_2 concentration ranging from 10 to 2000 ppb at room temperature. The 4NTP-MoS_2 exhibits an outstanding positive linear relationship between the response tested from 0.247 to 7.548 and the NO_2 concentration ranging from 10 to 2000 ppb (**Figure S1**), which is a much higher response than that of pristine MoS_2 (Fig. 3a). Furthermore, compared with the reported NO_2 gas sensors, the 4NTP-MoS_2 under illumination

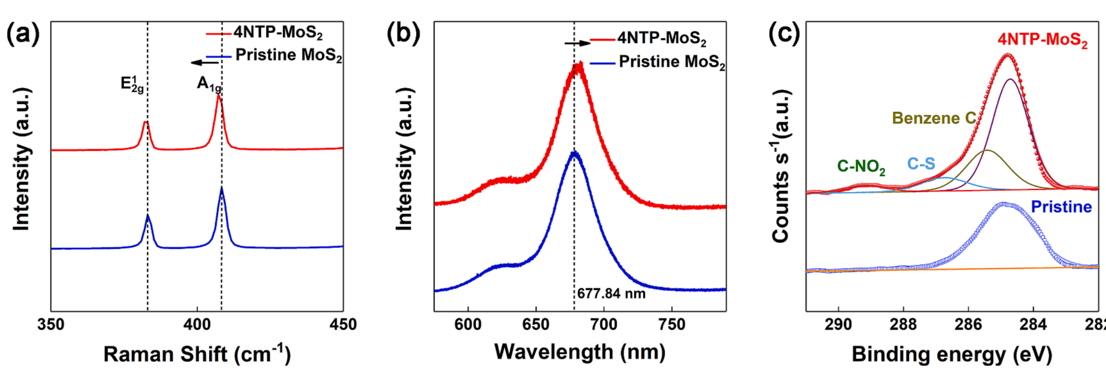

Fig. 2. The (a) Raman spectra, (b) comparison of photoluminescence (PL) spectra and (c) micro-area XPS spectra of C 1 s for the pristine MoS_2 (blue) and 4NTP-MoS_2 (red).

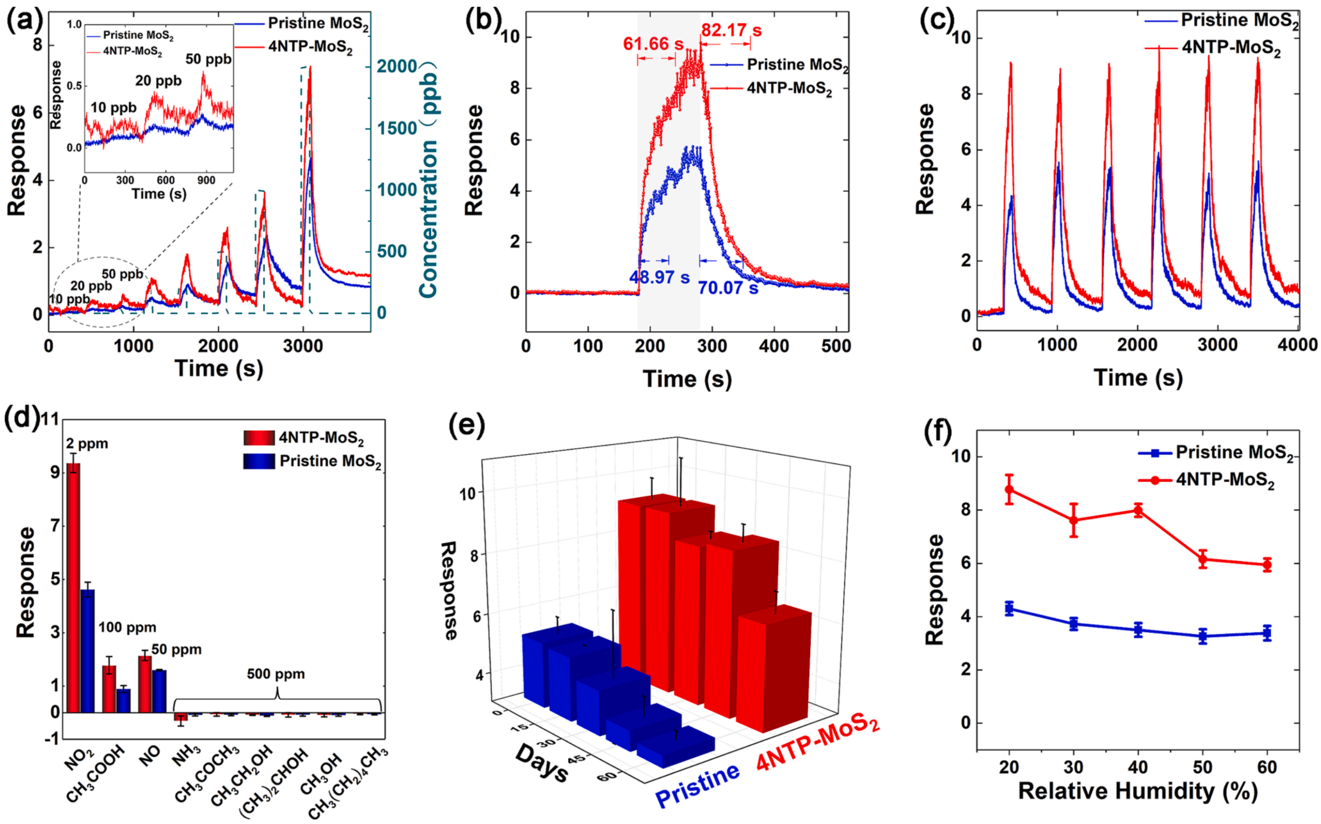

Fig. 3. Gas sensing performance of the pristine MoS_2 (blue) and 4NTP-MoS_2 (red) under 405 nm light illumination with a power density of 12 mW/cm^2. (a) Exposed to several NO_2 concentrations raising from 10 to 2000 ppb. (b) Dynamic response under 2 ppm NO_2 with a precise response/recovery time. (c) Six-cycle response curve exposed toward 2 ppm NO_2. (d) Selectivity of pristine MoS_2 and 4NTP-MoS_2 toward different gases. (e) Long-term stability from 0 to 60 days. (f) Humidity resistance response with the relative humidity increases linearly from 20 % to 60 %.

has an extremely low LOD of 10 ppb (50 ppb for pristine). In comparison with the pristine MoS_2, 4NTP-MoS_2 response increased by about 200 % and maintained quick response/recovery speed (Fig. 3**b**). The pristine MoS_2 and 4NTP-MoS_2 presented six successive response-recovery curves toward 2 ppm NO_2 with an average response of 5.198 and 9.148 (Fig. 3**c**), which performed good stability. Furthermore, the 4NTP healed devices inherit excellent selectivity of MoS_2 toward NO_2 among numerous gases including NO, NH_3, and acetic acid as illustrated in Fig. 3**d**. As shown in Fig. 3**e, 4NTP**-MoS_2 maintained 92.7 % of initial response after 45 days. Even after 60 days, an average response of 70.8 % was obtained, indicating reliable long-term stability of 4NTP-MoS_2. To explore the humidity effect on the gas sensing performance of pristine MoS_2 and 4NTP-MoS_2, the aforementioned gas sensors were exposed to different relative humidity (RH) from 20 % to 60 % and the corresponding gas sensing response toward 2 ppm NO_2 was recorded (Fig. 3**f**). We found that the 4NTP-MoS_2 performed high reliability when the RH was under 50 %. With the increment of RH both the pristine MoS_2 and 4NTP-MoS_2 performance would be suppressed and the same phenomena have also been reported in other NO_2 gas sensors.[49–51] Besides, to verify the impact of DMSO on MoS_2 performance, DMSO treated MoS_2 and pristine MoS_2 were tested under the same condition. As shown in **Figure S3**, the DMSO treated MoS_2 performed no difference from pristine MoS_2, indicating solvent has been completely evaporated.

3.3. Gas sensing mechanism

The NO_2 absorption mechanism of TMDCs has been systematically explored in our previous work.[48,52] It is noted that when NO_2 adsorbs to n-type MoS_2 the electrons correspondingly transfer from n-MoS_2 to NO_2, the reduction of majority carrier ultimately increased the resistance of n-MoS_2. To verify the adsorption capacity of TMDCs for NO_2 is enhanced after SVP, we analyzed the XPS spectra of pristine MoS_2 and 4NTP-MoS_2 (full spectral of XPS in **Figure S4**). As shown in Fig. 4a and b, SVP MoS_2 shows a prominent NO_2 absorption peak at 405–407 eV, [53,54] indicating that 4NTP-MoS_2 has a higher absorption ability to NO_2 than pristine MoS_2. KPFM was also adopted in situ to investigate the mechanism of NO_2 absorption and the gas sensing performance improvement of MoS_2 after 4NTP treatment. The surface potential also known as contact potential difference (CPD) is determined by the work function difference between the sample (W_{sample}) and the AFM tip (W_{tip}) (Equation (2)):

$$CPD = (W_{sample} - W_{tip})/e \tag{2}$$

where e is the elementary charge [39]. Fig. 4**c and d** show the KPFM images of MoS_2 nanosheets before and after the SVP respectively. Through semiquantitative analysis, the equivalent doping effect could help to understand the essence of SVP and NO_2 absorption. Firstly, as shown in Fig. 4**d and e**, the relative surface potential of the 4NTP-MoS_2 raised from −57.1 mV to –32.2 mV after NO_2 exposure, which indicates the Fermi level of the MoS_2 is shifted toward the valence band. From another aspect, when NO_2 gas is supplied, the NO_2 molecules will absorb on the surface of MoS_2 and extract electrons from MoS_2 [13,23] (**Figure S6**), indicating an n-doping effect on MoS_2. Secondly, the electron-withdrawing effect of nitro group on 4NTP could promote the sulfhydryl group to dissociate protons and form the corresponding 4NTP anion. Comparatively, the electron-donating group like amino group and methoxyl group could not facilitate this dissociation. The precise CPD and work function analysis of SVP in **Figure S5** is in line with our hypothesis. After MoS_2 was healed by 4NTP, the MoS_2 Fermi level shifted toward the conduction band, this phenomenon proved this SVP process is n-doping.

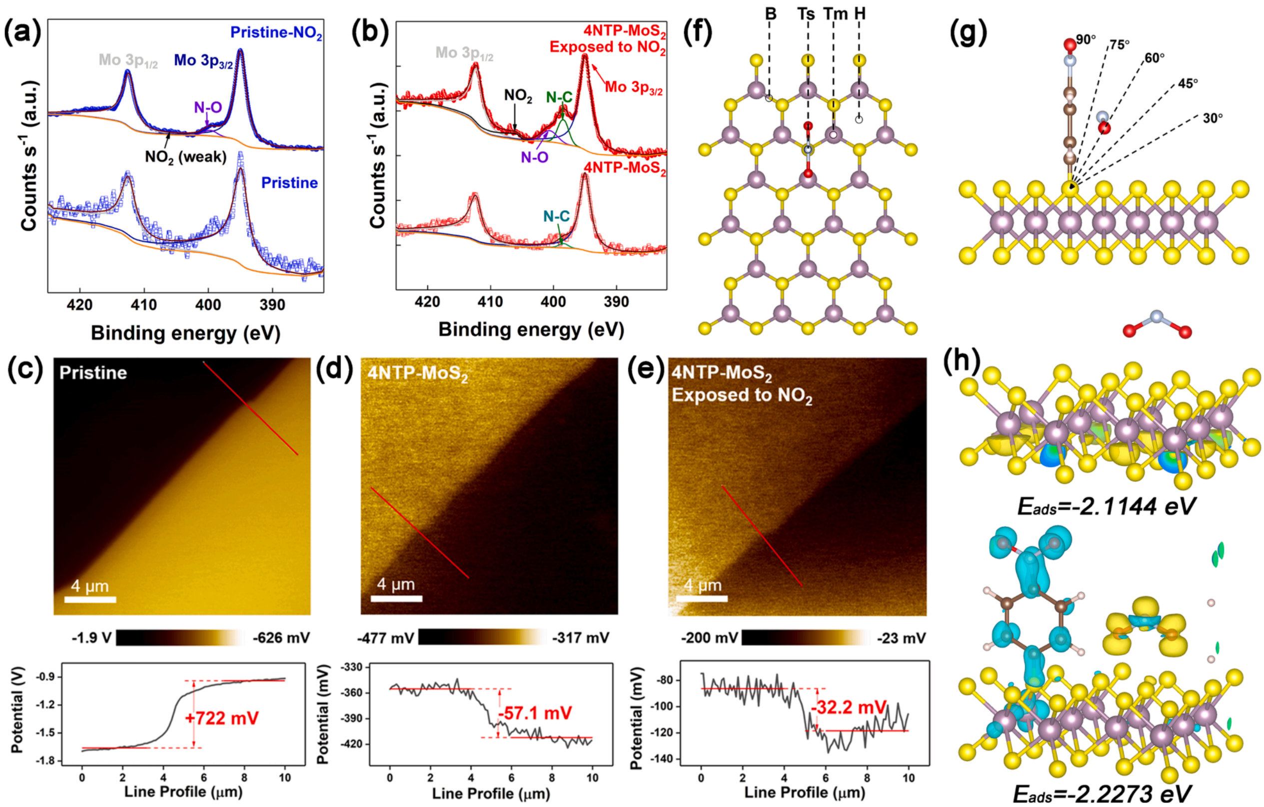

Fig. 4. Micro-area N 1 s XPS spectra of the (a) pristine (blue) and (b) 4NTP-MoS_2(red). KPFM images of the pristine MoS_2 (c), 4NTP-MoS_2 (d) and (e) 4NTP-MoS_2 exposed to NO_2. (f) Top view of MoS_2 model with 4 NO_2 adsorption sites. (g) Lateral view of MoS_2 model with 5 angles of 4NTP. (h) Charge density difference images of pristine and 4NTP-MoS_2.

The DFT models were calculated to elucidate the charge transfer among 4NTP, NO_2, and MoS_2. The MoS_2 nanosheet structure was built as a predominant interface region to interact with NO_2 molecules. The most quintessential four highly symmetric models were firstly considered (B for NO_2 on Mo-S bond, Ts for sulfur atom, Tm for Mo atom and H for hexagonal plane center). The adsorption energies of these NO_2 adsorption sites were calculated to obtain a stable adsorption model (**Table S1**) which confirmed that the model of NO_2 above the sulfur atom (Ts) possesses minimum energy (Fig. 4**f**). Another key factor for the adsorption model was the angle between MoS_2 and 4NTP. The angle between MoS_2 and 4NTP was adjusted to 30°, 45°, 60°, 75°, and 90° (NO_2 is placed at Ts site), respectively (Fig. 4**g**). The total energy of the system (E_{tot}) was calculated and 90° has the lowest E_{tot} (**Table S2**). Herein, we established and optimized a relatively stable model with the lowest E_{tot} when the NO_2 adsorption site is Ts and the angle between 4NTP and MoS_2 is 90°. As shown in Fig. 4**h**, the adsorption energy of MoS_2 for NO_2 increases from −2.1144 eV to −2.2273 eV after SVP, proving that the adsorption capacity of MoS_2 for NO_2 increased after vacancies repair. Besides, electrons tend to accumulate on NO_2 for 4NTP repaired MoS_2 according to the charge density difference diagram (the blue lobes represent charge depletion and yellow ones represent charge accumulation). In conclusion, the 4NTP-MoS_2 shows ultrahigh sensitivity toward NO_2 under room temperature owing to the *n*-doping 4NTP healing process increased the carriers of MoS_2 and promoted the electron transfer from MoS_2 to NO_2.

3.4. Universality test of TMDCs

To further prove the universality of the SVP method, we prepared 4NTP-WS_2, 4NTP-WSe_2, and 4NTP-$MoSe_2$ based gas sensors via the same preparation method of 4NTP-MoS_2 and monitored the response of NO_2 with concentration gradients of 0.5–10 ppm before and after sulfur vacancy patching. As shown in Fig. 5, the response of the above TMDCs-based gas sensors has been improved after vacancies repair using 4NTP. It is indicated that this vacancy repair method is also universal to other TMDCs and could be used to enhance the NO_2 adsorption of TMDCs.

In Table 1, we summarized the representative research of TMDCs-based room temperature NO_2 gas sensors in recent years. Compared with other types of TMDCs-based gas sensors, 4NTP-MoS_2 has good performance in response, response/recovery time, long-term stability, and humidity stability. It is worth noting that the 4NTP-MoS_2 has the lowest LOD among the reported TMDCs NO_2 gas sensors, which could contribute to the 4NTP dominated MoS_2 *n*-doping process.

4. Conclusion

In summary, we fabricated functionalized transition metal dichalcogenides through a sample solution process by 4-nitrothiophenol and systematically analyzed their gas sensing performance. Spectroscopic and surface analysis proved that 4-nitrothiophenol successfully healed MoS_2 through the formation of covalent bonds. The MoS_2 after sulfur vacancy patching showed higher gas sensing response (519 % to 914 %, 2 ppm), and lower detect limitation to NO_2 (50 ppb raise to 10 ppb). Through Kelvin probe force microscopy and density functional theory calculation, we attributed the phenomenon of enhanced gas response caused by sulfur vacancy patching to the enhancement of physical absorption of NO_2 and carrier mobility (*n*-type doping) after vacancy repair, which would raise the number of electrons transferred to NO_2. The sulfur vacancy patching approach we proposed offers a facile approach to modify the electrical property and improve gas sensing performance of transition metal dichalcogenides.

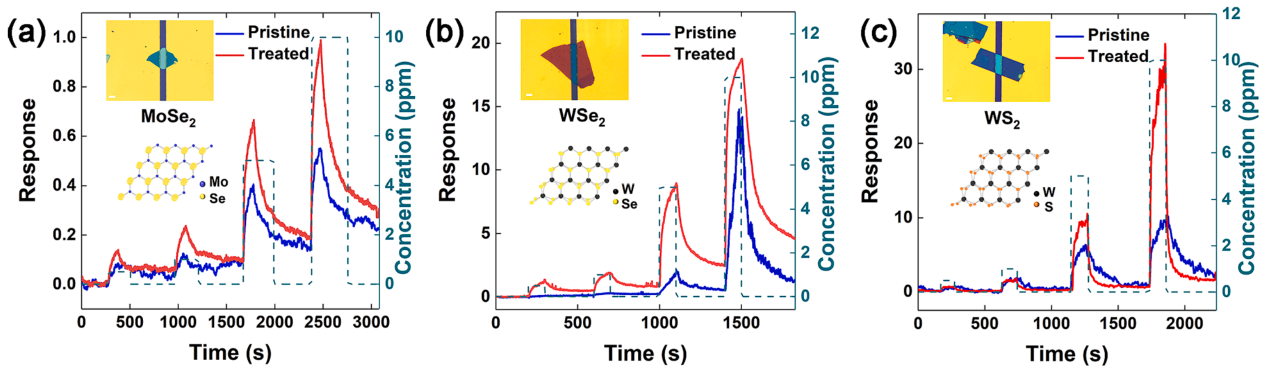

Fig. 5. Gas sensing performance of (a) $MoSe_2$, (b) WS_2 and (c) WSe_2-based gas sensors exposed to 0.5, 1, 5, and 10 ppm NO_2, under 405 nm light illumination with a power density of 12 mW/cm^2 (blue lines for pristine TMDCs and red lines for 4NTP treated TMDCs.

Table 1
Gas sensing performance of room-temperature TMDCs based NO_2 gas sensors.

Materials	Method	pLOD[a)] [ppb]	Concentration [ppm]	Response[#)] [%]	τ_{res}/τ_{rec} [b)] [s]	Wavelength[c)]
$MoSe_2$ [55]	Liquid Phase Exfoliation	None	5	40	~300/>1000	No
$MoTe_2$ [56]	Mechanical exfoliation	20	0.02	18	300/120	254 nm (2.5 mW/cm^2)
WS_2 [57]	Hydrothermal	100	0.1	9.3	~120 > 360	No
WSe_2 [58]	LPE	50	0.05	5	50/1050	No
ReS_2 [48]	Mechanical exfoliation	50	0.5	898	55/180	254 nm (2.5 mW/cm^2)
NbS_2 [59]	CVD	500	5	18	>2000	No
WS_2/PbS[60]	LPE	20	1	200	~300/~500	UV
MoS_2/WSe_2 [61]	Mechanical exfoliation	None	10	180	>1000	Solar (10 W/m^2)
MoS_2/SiO_2 NRs [62]	CVD	1000	50	400	~1000/>2000	No
$MoS_2@WS_2$ [63]	Hydrothermal	10	50	26.12	1.6/27.7	No
WS_2@CNFs [64]	Hydrothermal	31	10	250	54/305	No
$PtSe_2$/ML MOFs [65]	Mechanical exfoliation	None	5	45	>600	No
MoS_2-4NTP (This Work)	Mechanical exfoliation	10	2	900	61/82	405 nm (12 mW/cm^2)

[a)] pLOD for Practical limit of detection.
[b)] τ_{res} for Response time, τ_{rec} for Recovery time.
[c)] Wavelength refers to light wavelength illuminated on material.
[#)] For convenience of comparison, the evaluation of the response is converted as $Response = \frac{|I_g - I_a|}{I_a} \times 100(\%)$.

Author Contributions

X-C.L. and Y.N. contributed equally to this work. X-C.L. and Y.N conceived and designed the research; X-C.L. and D.J. carried out the experiments. Y.W., J-W.Z., Y-C.F., H.L., H-H.Y., Y-K.L., P.J.F. and G-F.Z. helped discuss the data and revise the manuscript; X-C.L., W-J.L. and L-R.W. conducted DFT calculations with the guidance of Z-P.H. and Y-C.F.; X-C.L. and Y.N. wrote the manuscript with input from all authors. All authors discussed revised and approved the manuscript.

CRediT authorship contribution statement

Xiangcheng Liu: Conceptualization, Methodology, Investigation, Writing – original draft. **Yue Niu:** Conceptualization, Resources, Writing – review & editing. **Duo Jin:** Validation, Investigation. **Junwei Zeng:** Writing – review & editing. **Wanjiang Li:** Investigation, Software. **Lirong Wang:** Investigation, Software. **Zhipeng Hou:** Resources. **Yancong Feng:** Supervision. **Hao Li:** Resources. **Haihong Yang:** Resources. **Yi-Kuen Lee:** Resources. **Paddy J. French:** Resources. **Yao Wang:** Supervision, Resources, Writing – review & editing. **Guofu Zhou:** Resources.

Declaration of Competing Interest

The authors declare that they have no known competing financial interests or personal relationships that could have appeared to influence the work reported in this paper.

Data availability

Data will be made available on request.

Acknowledgments

This work was supported by the National Natural Science Foundation of China (Grant No.51902109 and 51973070), Basic Research Program of Guangzhou (202201010546), Innovative Team Project of Education Bureau of Guangdong Province (2018KCXTD009), Science and Technology Program of Guangzhou (No.2019050001), Guangdong Science and Technology Project-International Cooperation (2022A0505050069), Guangdong Basic and Applied Basic Research Foundation (2022A1515010577), Startup Foundation from SCNU, Guangdong Provincial Key Laboratory of Optical Information Materials and Technology (2017B030301007), MOE International Laboratory for Optical Information Technologies, the 111 Project and Special Funds for the Cultivation of Guangdong college students' Scientific and Technological Innovation ("Climbing Program", pdjh2021b0136).

Appendix A. Supplementary material

Supplementary data to this article can be found online at https://doi.org/10.1016/j.jcis.2023.06.092.

References

[1] H. Qiao, H. Liu, Z. Huang, R. Hu, Q. Ma, J. Zhong, X. Qi, Tunable electronic and optical properties of 2D monoelemental materials beyond graphene for promising applications, Energy Environ. Mater. 4 (4) (2021) 522–543.

[2] H. Tang, L.N. Sacco, S. Vollebregt, H. Ye, X. Fan, G. Zhang, Recent advances in 2D/nanostructured metal sulfide-based gas sensors: mechanisms, applications, and perspectives, J. Mater. Chem. A 8 (47) (2020) 24943–24976.

[3] S. Manzeli, D. Ovchinnikov, D. Pasquier, O.V. Yazyev, A. Kis, 2D transition metal dichalcogenides, Nat. Rev. Mater. 2 (8) (2017) 1–15.

[4] Z. Hu, Z. Wu, C. Han, J. He, Z. Ni, W. Chen, Two-dimensional transition metal dichalcogenides: interface and defect engineering, Chem. Soc. Rev. 47 (9) (2018) 3100–3128.

[5] Y. Zhao, S. Bertolazzi, P. Samorì, A universal approach toward light-responsive two-dimensional electronics: chemically tailored hybrid van der Waals heterostructures, ACS Nano 13 (4) (2019) 4814–4825.

[6] Y. Zhao, M. Gobbi, L.E. Hueso, P. Samorì, Molecular approach to engineer two-dimensional devices for CMOS and beyond-CMOS applications, Chem. Rev. 122 (1) (2021) 50–131.

[7] F.J. Urbanos, S. Gullace, P. Samorì, MoS_2 Defect Healing for High-Performance Chemical Sensing of Polycyclic Aromatic Hydrocarbons, ACS Nano 16 (7) (2022) 11234–11243.

[8] J. Wang, Z. Ji, G. Yang, X. Chuai, F. Liu, Z. Zhou, C. Lu, W. Wei, X. Shi, J. Niu, Charge transfer within the F4TCNQ-MoS_2 van der Waals Interface: Toward electrical properties tuning and gas sensing application, Adv. Funct. Mater. 28 (51) (2018) 1806244.

[9] T. Tang, Z. Li, Y.F. Cheng, K. Xu, H.G. Xie, X.X. Wang, X.Y. Hu, H. Yu, B.Y. Zhang, X.W. Tao, Single-step growth of p-type 1D Se/2D $GeSe_xO_y$ heterostructures for optoelectronic NO_2 gas sensing at room temperature, J. Mater. Chem. A 11 (12) (2023) 6361–6374.

[10] X.X. Wang, Z. Li, Y. Yang, T. Tang, Y.F. Cheng, K. Xu, H.G. Xie, Y.L. Chen, L. Cheng, X.W. Tao, 3D Substoichiometric MoO_{3-x}/EGaln framework for room temperature NH_3 gas sensing, J. Alloys Compd. 168690 (2023).

[11] T. Tang, Z. Li, Y.F. Cheng, H.G. Xie, X.X. Wang, Y.L. Chen, L. Cheng, Y. Liang, X. Y. Hu, C.M. Hung, In-situ mechanochemically tailorable 2D gallium oxyselenide for enhanced optoelectronic NO_2 gas sensing at room temperature, J. Hazard. Mater. 451 (2023), 131184.

[12] D. Wang, D. Zhang, X. Chen, H. Zhang, M. Tang, J. Wang, Multifunctional respiration-driven triboelectric nanogenerator for self-powered detection of formaldehyde in exhaled gas and respiratory behavior, Nano Energy 102 (2022), 107711.

[13] D. Wang, D. Zhang, J. Guo, Y. Hu, Y. Yang, T. Sun, H. Zhang, X. Liu, Multifunctional poly (vinyl alcohol)/Ag nanofibers-based triboelectric nanogenerator for self-powered MXene/tungsten oxide nanohybrid NO_2 gas sensor, Nano Energy 89 (2021), 106410.

[14] K. Lee, R. Gatensby, N. McEvoy, T. Hallam, G.S. Duesberg, High-performance sensors based on molybdenum disulfide thin films, Adv. Mater. 25 (46) (2013) 6699–6702.

[15] J.-S. Kim, H.-W. Yoo, H.O. Choi, H.-T. Jung, Tunable volatile organic compounds sensor by using thiolated ligand conjugation on MoS_2, Nano Lett. 14 (10) (2014) 5941–5947.

[16] Y.H. Kim, J.S. Park, Y.-R. Choi, S.Y. Park, S.Y. Lee, W. Sohn, Y.-S. Shim, J.-H. Lee, C.R. Park, Y.S. Choi, Chemically fluorinated graphene oxide for room temperature ammonia detection at ppb levels, J. Mater. Chem. A 5 (36) (2017) 19116–19125.

[17] D.M. Sim, M. Kim, S. Yim, M.-J. Choi, J. Choi, S. Yoo, Y.S. Jung, Controlled doping of vacancy-containing few-layer MoS_2 via highly stable thiol-based molecular chemisorption, ACS Nano 9 (12) (2015) 12115–12123.

[18] D. Voiry, A. Goswami, R. Kappera, C.d.C.C.e. Silva, D. Kaplan, T. Fujita, M. Chen, T. Asefa, M. Chhowalla, Covalent functionalization of monolayered transition metal dichalcogenides by phase engineering, Nat. Chem. 7 (1) (2015) 45–49.

[19] S. Presolski, M. Pumera, Covalent functionalization of MoS_2, Mater. Today 19 (3) (2016) 140–145.

[20] Y. Wang, S.M. Gali, A. Slassi, D. Beljonne, P. Samorì, Collective dipole-dominated doping of monolayer MoS_2: Orientation and magnitude control via the supramolecular approach, Adv. Funct. Mater. 30 (36) (2020) 2002846.

[21] S.H. Amsterdam, T.K. Stanev, Q. Zhou, A.-J.-T. Lou, H. Bergeron, P. Darancet, M. C. Hersam, N.P. Stern, T.J. Marks, Electronic coupling in metallophthalocyanine–transition metal dichalcogenide mixed-dimensional heterojunctions, ACS Nano 13 (4) (2019) 4183–4190.

[22] S. Bertolazzi, M. Gobbi, Y. Zhao, C. Backes, P. Samori, Molecular chemistry approaches for tuning the properties of two-dimensional transition metal dichalcogenides, Chem. Soc. Rev. 47 (17) (2018) 6845–6888.

[23] H.G. Ji, P. Solís-Fernández, D. Yoshimura, M. Maruyama, T. Endo, Y. Miyata, S. Okada, H. Ago, Chemically tuned p-and n-type WSe_2 monolayers with high carrier mobility for advanced electronics, Adv. Mater. 31 (42) (2019) 1903613.

[24] M. Vera-Hidalgo, E. Giovanelli, C. Navio, E.M. Perez, Mild covalent functionalization of transition metal dichalcogenides with maleimides: A "click" reaction for 2H-MoS_2 and WS_2, J. Am. Chem. Soc. 141 (9) (2019) 3767–3771.

[25] H. Im, A. Bala, B. So, Y.J. Kim, S. Kim, Customization of MoS_2 phototransistors via thiol-based functionalization, Adv. Electron. Mater. 7 (11) (2021) 2100644.

[26] R.H. Gonçalves, R. Fiel, M.R. Soares, W.H. Schreiner, C.M. Silva, E.R. Leite, Single-step exfoliation and covalent functionalization of MoS_2 nanosheets by an organosulfur reaction, Chem. Eur. J. 21 (44) (2015) 15583–15588.

[27] K.C. Knirsch, N.C. Berner, H.C. Nerl, C.S. Cucinotta, Z. Gholamvand, N. McEvoy, Z. Wang, I. Abramovic, P. Vecera, M. Halik, Basal-plane functionalization of chemically exfoliated molybdenum disulfide by diazonium salts, ACS Nano 9 (6) (2015) 6018–6030.

[28] M. Makarova, Y. Okawa, M. Aono, Selective adsorption of thiol molecules at sulfur vacancies on MoS_2 (0001), followed by vacancy repair via S-C dissociation, J. Phys. Chem. C 116 (42) (2012) 22411–22416.

[29] S. Bertolazzi, S. Bonacchi, G. Nan, A. Pershin, D. Beljonne, P. Samorì, Engineering chemically active defects in monolayer MoS_2 transistors via ion-beam irradiation and their healing via vapor deposition of alkanethiols, Adv. Mater. 29 (18) (2017) 1606760.

[30] M.A. Gerkman, J.K. Lee, X. Li, Q. Zhang, M. Windley, M.V. Fonseca, Y. Lu, J. H. Warner, G.G. Han, Direct imaging of individual molecular binding to clean nanopore edges in 2D monolayer MoS_2, ACS Nano 14 (1) (2019) 153–165.

[31] E.P. Nguyen, B.J. Carey, J.Z. Ou, J. van Embden, E.D. Gaspera, A.F. Chrimes, M. J. Spencer, S. Zhuiykov, K. Kalantar-zadeh, T. Daeneke, Electronic tuning of 2D MoS_2 through surface functionalization, Adv. Mater. 27 (40) (2015) 6225–6229.

[32] S. Ippolito, A.G. Kelly, R. Furlan de Oliveira, M.-A. Stoeckel, D. Iglesias, A. Roy, C. Downing, Z. Bian, L. Lombardi, Y.A. Samad, Covalently interconnected transition metal dichalcogenide networks via defect engineering for high-performance electronic devices, Nat. Nanotechnol. 16 (5) (2021) 592–598.

[33] H. Jiang, L. Cao, Y. Li, W. Li, X. Ye, W. Deng, X. Jiang, G. Wang, G. Xu, Organic "receptor" fully covered few-layer organic–metal chalcogenides for high-performance chemiresistive gas sensing at room temperature, Chem. Commun. 56 (40) (2020) 5366–5369.

[34] Y. Niu, R. Frisenda, E. Flores, J.R. Ares, W. Jiao, D. Perez de Lara, C. Sanchez, R. Wang, I.J. Ferrer, A. Castellanos-Gomez, Polarization-sensitive and broadband photodetection based on a mixed-dimensionality TiS_3/Si p-n junction, Adv. Opt. Mater. 6 (19) (2018) 1800351.

[35] H.G. Ji, Y.-C. Lin, K. Nagashio, M. Maruyama, P. Solís-Fernández, A. Sukma Aji, V. Panchal, S. Okada, K. Suenaga, H. Ago, Hydrogen-assisted epitaxial growth of monolayer tungsten disulfide and seamless grain stitching, Chem. Mater. 30 (2) (2018) 403–411.

[36] S. Pak, S. Jang, T. Kim, J. Lim, J.S. Hwang, Y. Cho, H. Chang, A.R. Jang, K.H. Park, J. Hong, Electrode-induced self-healed monolayer MoS_2 for high performance transistors and phototransistors, Adv. Mater. 33 (41) (2021) 2102091.

[37] L.-J. Wan, M. Terashima, H. Noda, M. Osawa, Molecular orientation and ordered structure of benzenethiol adsorbed on gold (111), J. Phys. Chem. B 104 (15) (2000) 3563–3569.

[38] M. Mantina, A.C. Chamberlin, R. Valero, C.J. Cramer, D.G. Truhlar, Consistent van der Waals radii for the whole main group, J. Phys. Chem. A 113 (19) (2009) 5806–5812.

[39] L. Daukiya, J. Teyssandier, S. Eyley, S. El Kazzi, M.C.R. Gonzalez, B. Pradhan, W. Thielemans, J. Hofkens, S. De Feyter, Covalent functionalization of molybdenum disulfide by chemically activated diazonium salts, Nanoscale 13 (5) (2021) 2972–2981.

[40] C.R. Ryder, J.D. Wood, S.A. Wells, Y. Yang, D. Jariwala, T.J. Marks, G.C. Schatz, M. C. Hersam, Covalent functionalization and passivation of exfoliated black phosphorus via aryl diazonium chemistry, Nat. Chem. 8 (6) (2016) 597–602.

[41] Y. Li, C.-Y. Xu, P. Hu, L. Zhen, Carrier control of MoS_2 nanoflakes by functional self-assembled monolayers, ACS Nano 7 (9) (2013) 7795–7804.

[42] D. Wang, D. Zhang, Q. Pan, T. Wang, F. Chen, Gas sensing performance of carbon monoxide sensor based on rod-shaped tin diselenide/MOFs derived zinc oxide polyhedron at room temperature, Sensors Actuators B: Chem. 371 (2022), 132481.

[43] H. Nan, Z. Wang, W. Wang, Z. Liang, Y. Lu, Q. Chen, D. He, P. Tan, F. Miao, X. Wang, Strong photoluminescence enhancement of MoS_2 through defect engineering and oxygen bonding, ACS Nano 8 (6) (2014) 5738–5745.

[44] N. Zhou, R. Wang, X. Zhou, H. Song, X. Xiong, Y. Ding, J. Lü, L. Gan, T. Zhai, P-GaSe/N-MoS_2 vertical heterostructures synthesized by van der Waals epitaxy for photoresponse modulation, Small 14 (7) (2018) 1702731.

[45] D. Wang, D. Zhang, Q. Mi, A high-performance room temperature benzene gas sensor based on $CoTiO_3$ covered TiO_2 nanospheres decorated with Pd nanoparticles, Sens. Actuators B: Chem. 350 (2022), 130830.

[46] D. Wang, D. Zhang, Y. Yang, Q. Mi, J. Zhang, L. Yu, Multifunctional latex/polytetrafluoroethylene-based triboelectric nanogenerator for self-powered organ-like MXene/metal-organic framework-derived CuO nanohybrid ammonia sensor, ACS Nano 15 (2) (2021) 2911–2919.

[47] J. Schobing, V. Tschamber, A. Brillard, G. Leyssens, Impact of biodiesel impurities on carbon oxidation in passive regeneration conditions: Influence of the alkali metals, Appl. Catal., B 226 (2018) 596–607.

[48] J. Zeng, Y. Niu, Y. Gong, Q. Wang, H. Li, A. Umar, N.F. de Rooij, G. Zhou, Y. Wang, All-dry transferred ReS_2 nanosheets for ultrasensitive room-temperature NO_2 sensing under visible light illumination, ACS Sens. 5 (10) (2020) 3172–3181.

[49] F. Qu, S. Zhang, C. Huang, X. Guo, Y. Zhu, T. Thomas, H. Guo, J.P. Attfield, M. Yang, Surface functionalized sensors for humidity-independent gas detection, Angew. Chem. 133 (12) (2021) 6635–6640.

[50] J.W. Yoon, J.S. Kim, T.H. Kim, Y.J. Hong, Y.C. Kang, J.H. Lee, A new strategy for humidity independent oxide chemiresistors: dynamic self-refreshing of In_2O_3

sensing surface assisted by layer-by-layer coated CeO_2 nanoclusters, Small 12 (31) (2016) 4229–4240.
[51] Z. Yang, D. Zhang, H. Chen, MOF-derived indium oxide hollow microtubes/MoS_2 nanoparticles for NO_2 gas sensing, Sens. Actuators B: Chem. 300 (2019), 127037.
[52] Y. Niu, J. Zeng, X. Liu, J. Li, Q. Wang, H. Li, N.F.D. Rooij, Y. Wang, G. Zhou, A photovoltaic self-powered gas sensor based on all-dry transferred MoS_2/GaSe Heterojunction for ppb-Level NO_2 sensing at room temperature, Adv. Sci. 8 (14) (2021) 2100472.
[53] K. Roodenko, M. Gensch, J. Rappich, K. Hinrichs, N. Esser, R. Hunger, Time-resolved synchrotron XPS monitoring of irradiation-induced nitrobenzene reduction for chemical lithography, J. Phys. Chem. B 111 (26) (2007) 7541–7549.
[54] J. Baltrusaitis, P.M. Jayaweera, V.H. Grassian, XPS study of nitrogen dioxide adsorption on metal oxide particle surfaces under different environmental conditions, PCCP 11 (37) (2009) 8295–8305.
[55] S. Zhang, T.H. Nguyen, W. Zhang, Y. Park, W. Yang, Correlation between lateral size and gas sensing performance of $MoSe_2$ nanosheets, Appl. Phys. Lett. 111 (16) (2017), 161603.
[56] E. Wu, Y. Xie, B. Yuan, H. Zhang, X. Hu, J. Liu, D. Zhang, Ultrasensitive and fully reversible NO_2 gas sensing based on p-type $MoTe_2$ under ultraviolet illumination, ACS Sens. 3 (9) (2018) 1719–1726.
[57] T. Xu, Y. Liu, Y. Pei, Y. Chen, Z. Jiang, Z. Shi, J. Xu, D. Wu, Y. Tian, X. Li, The ultra-high NO_2 response of ultra-thin WS_2 nanosheets synthesized by hydrothermal and calcination processes, Sensors Actuators B: Chem. 259 (2018) 789–796.
[58] R. Guo, Y. Han, C. Su, X. Chen, M. Zeng, N. Hu, Y. Su, Z. Zhou, H. Wei, Z. Yang, Ultrasensitive room temperature NO_2 sensors based on liquid phase exfoliated WSe_2 nanosheets, Sensors Actuators B: Chem. 300 (2019), 127013.
[59] Y. Kim, K.C. Kwon, S. Kang, C. Kim, T.H. Kim, S.-P. Hong, S.Y. Park, J.M. Suh, M.-J. Choi, S. Han, Two-dimensional NbS_2 gas sensors for selective and reversible NO_2 detection at room temperature, ACS Sens. 4 (9) (2019) 2395–2402.
[60] X. Chen, J. Hu, P. Chen, M. Yin, F. Meng, Y. Zhang, UV-light-assisted NO_2 gas sensor based on WS_2/PbS heterostructures with full recoverability and reliable anti-humidity ability, Sensors Actuators B: Chem. 339 (2021), 129902.
[61] Y. Kim, S. Lee, J.G. Song, K.Y. Ko, W.J. Woo, S.W. Lee, M. Park, H. Lee, Z. Lee, H. Choi, 2D transition metal dichalcogenide heterostructures for p-and n-type photovoltaic self-powered gas sensor, Adv. Funct. Mater. 30 (43) (2020) 2003360.
[62] Y.-S. Shim, K.C. Kwon, J.M. Suh, K.S. Choi, Y.G. Song, W. Sohn, S. Choi, K. Hong, J.-M. Jeon, S.-P. Hong, Synthesis of numerous edge sites in MoS_2 via SiO_2 nanorods platform for highly sensitive gas sensor, ACS Appl. Mater. Interfaces 10 (37) (2018) 31594–31602.
[63] M. Ikram, L. Liu, Y. Liu, L. Ma, H. Lv, M. Ullah, L. He, H. Wu, R. Wang, K. Shi, Fabrication and characterization of a high-surface area MoS_2@WS_2 heterojunction for the ultra-sensitive NO_2 detection at room temperature, J. Mater. Chem. A 7 (24) (2019) 14602–14612.
[64] Y. Xu, J. Xie, Y. Zhang, F. Tian, C. Yang, W. Zheng, X. Liu, J. Zhang, N. Pinna, Edge-enriched WS_2 nanosheets on carbon nanofibers boosts NO_2 detection at room temperature, J. Hazard. Mater. 411 (2021), 125120.
[65] S.R. Cho, D.H. Kim, M. Jeon, P. Rani, M. Gyeon, Y. Kim, M.K. Jo, S. Song, J.Y. Park, J. Kim, Overlaying monolayer metal-organic framework on $PtSe_2$-based gas sensor for tuning selectivity, Adv. Funct. Mater. 32 (47) (2022) 2207265.